

Computer Tomography of the Density and its Spatial Distribution of Wood-Plastic Composites

Yu Han,[†] Jinxing Ta,[†] and Dawei Qi *

The density and its spatial distribution of wood-plastic composites (WPCs) were tested by the computer tomography (CT) method. Based on the correlation among the attenuation coefficient, density, and CT number, a mathematical model between CT number and density of WPCs was established. This contributed to the realization of fast and nondestructive detection of WPC density and to the determination of the quality of wood-plastic composite products. Taking pine and poplar wood powder WPCs as subjects, the density was higher near the edge and lower in the middle of the sample, which resembled a "V" shape in the width direction. Compared with the density variations of poplar wood powder WPCs, those of pine wood powder had more of a "V" distribution.

Keywords: Wood-plastic composites; CT testing; CT number; Nondestructive detection; Density distribution

Contact information: School of Science, Northeast Forestry University, Harbin, 150040, P. R. China;

[†] These authors contributed to the work equally and should be regarded as co-first authors;

* Corresponding author: qidw9806@126.com

INTRODUCTION

Wood-plastic composites (WPCs) are materials that take plant fiber (wood powder, *Platycodon grandiflorum*, etc.) and plastic (polyethylene, polyvinyl chloride, etc.) as raw materials, and are made with plastic production technology in fixed proportions. The good mechanical properties of wood are not only retained, but the disadvantages of low strength and high variability are removed. Additionally, WPCs can be recycled and toxic substances are not easy to produce in the production process (Petchwattana *et al.* 2012). Therefore, WPCs are known as promising "green materials" (Clemons 2002; Pritchard 2004; Yang *et al.* 2015). Experts predict that WPCs will become one of the world's most important wood materials. WPCs have distinguished applications in many different spheres, e.g., automotive industries, windows, doors, and decking (Ashori 2008; Caufield *et al.* 2010), and have become very popular in Europe and the United States (Clemons 2002; Stark and Matuana 2007). WPCs have also been widely exploited in outdoor applications, e.g., public facilities and industrial or recreational purposes.

Many studies have been conducted by modifying the components or the percentages of WPCs (Adhikary *et al.* 2008; Khanjanzadeh *et al.* 2011). For example, Adhikary *et al.* (2008) noted that recycled HDPE and wood sawdust can be successfully applied to produce stable and strong WPCs. High dimensional stability and mechanical properties of composites can be achieved by improving the polymer content or by addition of coupling agents. These WPCs are made using either recycled or virgin high-density polyethylene (HDPE), with wood flour (*Pinus radiata*) as filler. In addition, some studies have concentrated on the influence of external conditions on WPCs. Specifically, a comparative analysis of the photostabilizing effects of hindered amine light

stabilizers (HALSs), an ultraviolet absorber (UVA), and zinc borate (ZnB) on WPCs was carried out to show the influence of accelerated weathering on the surface degradation and loss mechanical properties of treated WPCs (Li *et al.* 2014). Additionally, various technical means have been adopted in the experiments. The morphology of the WF-plastic interaction was investigated through SEM images. SEM images confirmed the degradation in mechanical properties of the WPCs. Increasing the plastic contents to more than 50% can significantly improve the resistance of WPCs to weathering (Yang *et al.* 2015). X-ray diffraction (XRD) analysis of composites with 3% and 5% nanoclay content has also been conducted. The effects of organoclay platelet contents (0, 3, and 5 wt%) and polypropylene type (virgin and recycled) on the mechanical properties of polypropylene/wood flour composites were investigated (Khanjanzadeh *et al.* 2011). In addition to mechanical properties, other characteristics of WPCs are also affected. The flexural properties, impact strength, density, and water uptake have been measured (TabkhPaz *et al.* 2013). However, there has been no emphasis on the method of density measurement in these studies.

Ideally the performance of WPCs should be determined by a nondestructive testing method. In recent years, with the continuous progress of science and technology, non-destructive testing technology has been developed by leaps and bounds (Yang and Qi 2011). Some widely used non-destructive testing methods include microwave detection, ultrasonic detection, optical detection, mechanical performance testing, nuclear magnetic resonance detection, and X-ray detection. X-ray detection technology is the most widely used. It is also important to note that computer tomography (CT) is a non-destructive testing method based on X-ray detection technology. CT is being increasingly utilized for automated detection and localization of internal defects in logs prior to scanning (Atanassov *et al.* 1983). Of all methods, CT has attracted considerable interest for industrial log inspection because of its internal imaging capacity, high penetrating power, efficiency, and resolution (Sarigul *et al.* 2003; Bhandarkar *et al.* 2005). It is reasonable to expect that CT is valid not only for the testing of logs, but also for the testing of WPCs. However, to date, there has been very little research conducted on the CT testing of density measurement and distribution of WPCs.

The main purpose of this paper is to use CT to scan WPCs and obtain their fault images. At the same time, the CT numbers of the reconstructed images were achieved and quantitative calculations were performed *via* the CT numbers. A mathematical model between CT number and density of WPCs was established, which was based on correlation between the CT number, material attenuation coefficient, and material density. Furthermore, the density and spatial distribution of WPCs were acquired. Assessment of quality levels of WPC products can be made by the density distribution available, and it is worth noting that the WPCs were undamaged.

STRUCTURE OF CT SCANNING SYSTEM AND IMAGING PRINCIPLE

Structure of CT Scanning System

Three radiation sources are generally employed in CT scanning: a low-energy X-ray source, γ -ray source, and high-energy X-ray source. As shown in Fig. 1, the X-ray CT system has five parts: the radiation source, mechanical scanning system, data acquisition system, display system, and storing system. The CT system is composed of two large parts, the imaging and computer segments.

The role of the mechanical scanning system is to rotate and translate the detected object while scanning and to adjust the distance and relative position between radiation source, object, and detector. A diagram of the mechanical system is displayed in Fig. 2. The main performance indices of the mechanical scanning system are the scanning mode, shift mode, controlling mode, and accuracy.

The key component of data acquisition system is the detector, which receives ray signals and forms the original data of the CT system. The performance of the detector directly affects the CT image quality.

Exploiting specific software in the computer system, many of the most important processes can be completed, including parameter adjusting, scanning procedure controlling, data processing, image reconstructing, image display, and storage. The main functions of the computer system are processing and controlling.

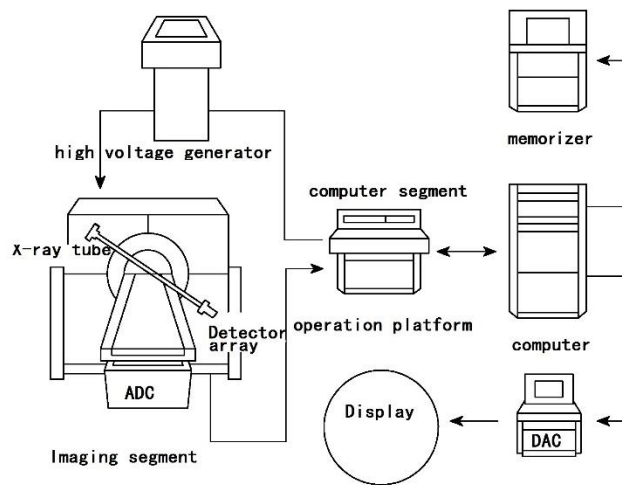


Fig. 1. Diagram of CT scanning system

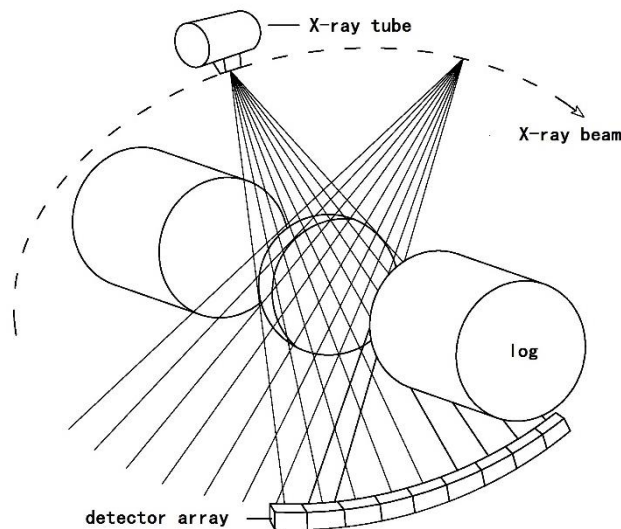


Fig. 2. Diagram of mechanical system

Basic Imaging Principles of CT

The imaging principles vary when various energy sources are used as the radiation source in CT scanning. Take X-rays for example; during CT scanning, an X-ray beam passes through the targeted part of the sample by multiple array projection around the sample, and a cross-sectional image or matrix is reconstructed. Each of these through the sample consists of an array of pixels (picture elements), which describes the X-ray attenuation coefficient of volume elements (voxels) of the scanned object. Thus, the attenuation coefficient can be correlated to the density of the voxel in a certain area of the object. The outputs of the CT scanner are matrices of CT numbers expressed in Hounsfield units (HU).

X-ray attenuation obeys Beer’s law. An attenuation illustration of Beer’s law is shown in Fig. 3. When a ray casts the object, ray intensity I can be expressed as:

$$I = I_0 e^{-\mu_1 d} \tag{1}$$

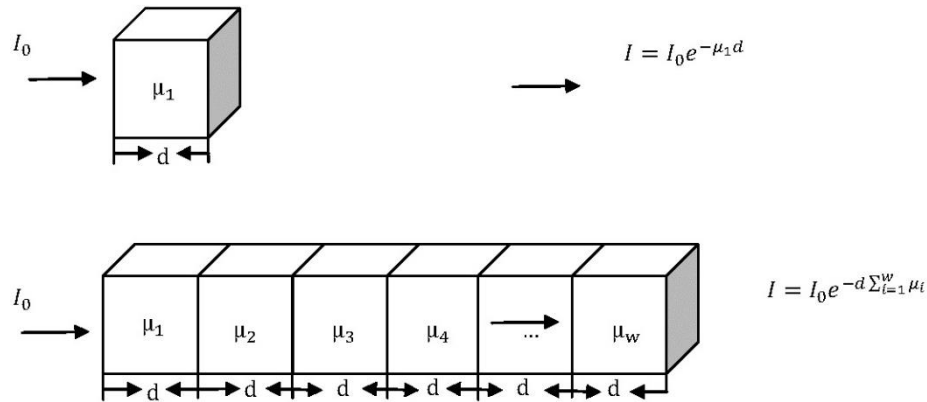


Fig. 3. Attenuation illustration of Beer law

When the object is heterogeneous, the ray intensity expression is written as:

$$I = I_0 e^{-d \sum_{i=1}^w \mu_i} \tag{2}$$

where I represents the ray intensity after attenuation occurs, I_0 denotes the initial ray intensity, μ_i indicates ray attenuation parameters of diverse objects, and d is the length of every detected object.

Calculation and Conversion of CT Number

CT number is the value of each pixel in the reconstructed image. It is a relative value in practical applications. The attenuation coefficient of water serves as a reference value. The calculation formula of CT number is as follows,

$$CT\ number = \frac{\mu_r - \mu_w}{\mu_w} \times k \tag{3}$$

where μ_r indicates the absorption coefficient of the tested object, μ_w denotes the absorption coefficient of water, and k represents a constant ($k = 1000$). The unit of CT number is Hounsfield units (Hu). The CT number of water is 0 in the formula. The CT

number of a vacuum is -1000. Figure 4 is the conversion graph for CT number. The point to emphasize here is that the conversion to CT number is an important procedure in the image reconstruction.

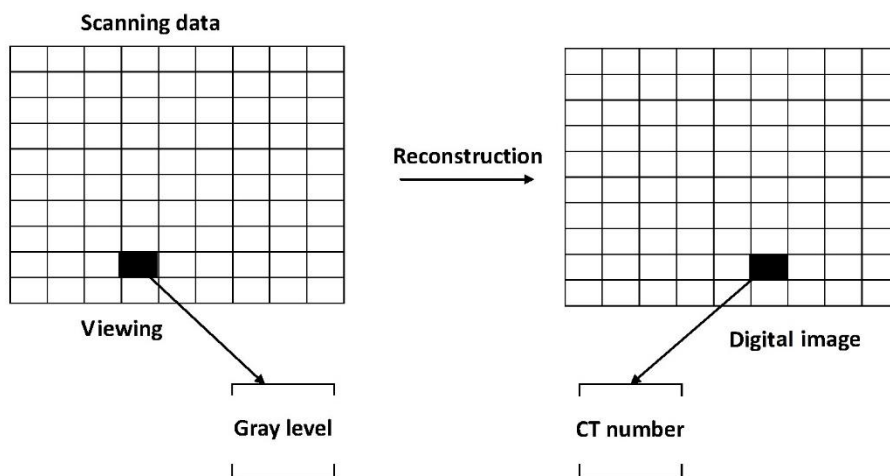


Fig. 4. The conversion to CT number

EXPERIMENTAL

Materials and Methods for Density Measurement

The WPCs used were double screw extrusion molded, provided by the Material Science and Technology Key Laboratory of the Ministry of Education of Northeast Forestry University. Cross-sectional scanning for a host of WPCs including pine and poplar wood powder WPCs was conducted (a total of 80). The scanning conditions of WPC samples are given. Philips Brilliance 64 channel spiral CT scanner of Philips's company (Cleveland, USA) was used. Scanning voltage and current were 100 KV and 80 mA, respectively. The sample was 200 mm long, 100 mm wide, and 20 mm thick. The ratio of wood powder to plastic was 3:2. Extrusion molding style was randomly selected. Tomography width was 5 mm. The total number of scanned layers equaled 20. The average CT number and density of 12 pieces of samples are displayed by Table 1.

The CT numbers of all cross-sectional images were obtained and recorded. Twelve pieces of WPCs were randomly selected. First, each piece was scanned with CT and the corresponding CT number was recorded. The average value of CT numbers was calculated.

Note that when the CT number was recorded, the selection of CT number should ignore corresponding values of defect sites and choose corresponding values of the uniform parts. Second, according to GB/T 17657 (1999), there are two methods for density measurement, the direct measuring and drainage method, we use the former. The density of WPCs is equal to the ratio of mass to volume and then the density was determined.

Materials and Methods for Measuring Density Distribution

Poplar and pine wood powder WPCs in the single screw extrusion molding style were selected. Two kinds of WPCs were scanned in cross-sectional mode, and corresponding images were saved. CT numbers of the entire images were achieved and marked in numerical way.

RESULTS AND DISCUSSION

Equation 3 represents the relationship between CT number and ray attenuation coefficient of WPCs. It may be accepted that the attenuation of WPCs is certainly correlated with the density. The reason is that exploiting CT number not only indicates the absorption and attenuation coefficient of materials but also indicates the relative relationship of different density tissues (Yu and Lu 2005). Therefore, it is proposed that the CT number of WPCs may also be associated with the corresponding density. Given the same controlled conditions, the magnitude of the average CT number can signify densities of the samples are different.

Table 1. Average CT Number and Corresponding Average Density

Sample number	Average CT number (Hu)	Average density (g/cm ³)
S1	141	1.214
S2	187	1.261
S3	446	1.411
S4	592	1.470
S5	359	1.419
S6	480	1.420
S7	500	1.436
S8	-11	1.000
S9	-83	0.957
S10	-30	0.977
S11	61	1.078
S12	50	1.076

The data given in Table 1 were analyzed and a mathematical model was successfully established, as follows,

$$y = 1.0420 + 8.2305 \times 10^{(-4)} x \quad (4)$$

where y indicates sample density and x denotes the CT number of sample faults or tomography. The coefficient is determined by the data in combination with the linear fitting formula. The relationship between CT number and density is shown in Fig. 5. The CT number distribution appears to be well correlated with density distribution for WPCs.

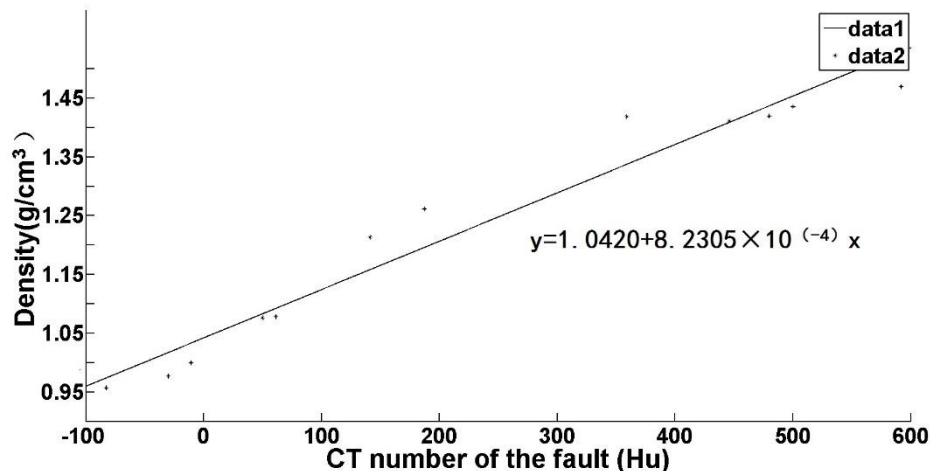


Fig. 5. Relationship between CT number and density of WPC faults

Table 2. CT Numbers of Cross Section of Pine Powder WPCs

Selection points Section	1	2	3	4	5	6	7	8	9	10
1	260	152	123	70	-19	-11	-47	51	136	221
2	266	172	123	79	-20	-17	-32	35	132	218
3	269	183	115	60	7	0	-61	51	137	203
4	258	186	129	66	-11	-9	-20	57	123	186
5	267	175	129	70	-29	-4	-38	48	113	203
6	163	127	65	-51	-16	20	18	110	179	199
7	190	120	66	-61	-26	-3	18	113	171	202
8	187	120	69	-16	-30	-41	28	109	192	185
9	194	131	52	-35	-4	-46	12	105	177	187
10	180	134	50	-53	-31	-13	28	107	182	175
11	195	122	32	-46	-43	-43	41	101	159	197
12	201	134	31	-39	-6	-20	61	88	181	180
13	201	129	42	-51	-17	-44	35	82	178	197
14	204	127	53	-36	-7	-66	-9	86	163	202
15	185	110	47	-59	-53	-10	3	74	182	207
16	195	120	42	-19	-43	-23	12	75	165	216
17	203	119	36	-31	-65	-38	-2	75	159	203
18	210	97	32	-32	-12	-11	12	77	152	216
19	213	118	31	-29	-45	-26	12	63	157	235
20	202	105	47	-35	-22	-16	24	76	148	234
Average value	212	134	66	-12	-25	-21	5	79	159	203

Table 3. CT Numbers of Cross Section of Poplar Powder WPCs

Selection points Section	1	2	3	4	5	6	7	8	9	10
1	212	141	131	107	105	113	113	143	134	212
2	218	159	161	136	92	100	92	176	170	218
3	190	160	156	135	101	116	120	112	162	190
4	203	125	130	108	90	135	138	142	145	203
5	179	178	162	140	113	112	156	172	169	179
6	200	188	156	149	140	124	115	156	147	203
7	185	161	158	143	124	99	179	185	200	243
8	222	164	159	151	134	93	182	193	207	222
9	207	196	187	180	178	149	169	181	211	220
10	203	203	156	140	171	136	113	146	178	212
11	243	180	171	116	95	130	148	149	150	212
12	193	177	170	134	109	137	189	187	212	218
13	211	175	152	145	97	156	167	166	180	190
14	203	163	151	148	129	154	174	169	178	203
15	218	192	172	141	101	158	154	179	182	179
16	200	186	142	182	136	196	153	139	214	147
17	212	158	167	133	109	137	218	158	206	185
18	183	180	153	171	161	177	180	200	215	222
19	196	194	173	170	95	159	198	202	207	220
20	211	191	156	145	131	176	187	187	190	222
average value	204	173	158	143	120	137	157	167	182	205

CT numbers of cross sections of pine and poplar wood powder WPCs are listed in Tables 2 and 3, respectively. Selected ten points were equally spaced at each fault of two kinds of WPCs. The total number of selected CT numbers amounts to 200 in each table.

It is known that the density distribution of a material reflects whether or not the density is uniform. Therefore, to intuitively analyze density distribution and enable better judgment of density uniformity, the CT number distribution of WPC sections is demonstrated in stereograph and line graph style (Figs. 6 to 9). As shown in Figs. 6 to 9, the section densities of pine and poplar powder WPCs exhibit distinct and regular changes in the width. To be specific, density is high near the edge and is low in the middle, showing a "V" shape. A comparison of the results obtained for these two materials suggests the density change of pine powder WPCs is more pronounced than that of poplar powder WPCs.

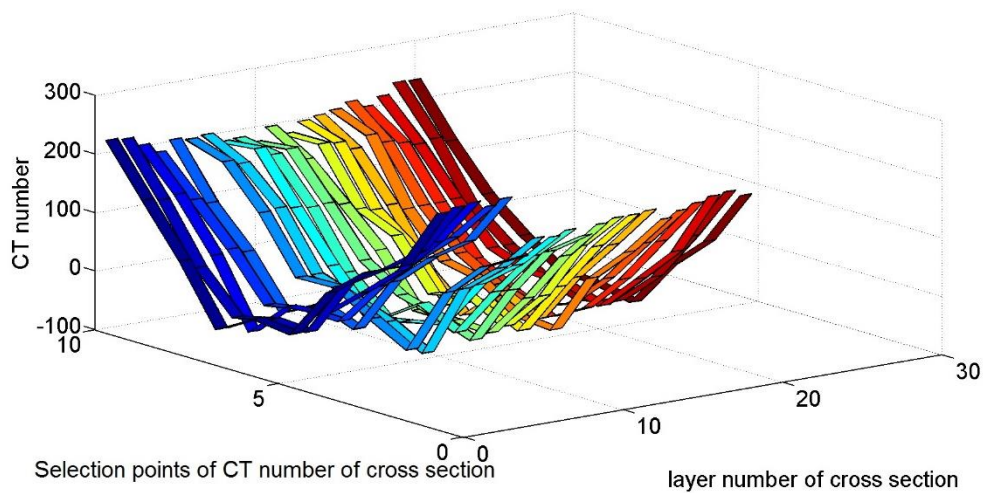


Fig. 6. Density spatial distribution of pine wood powder WPCs

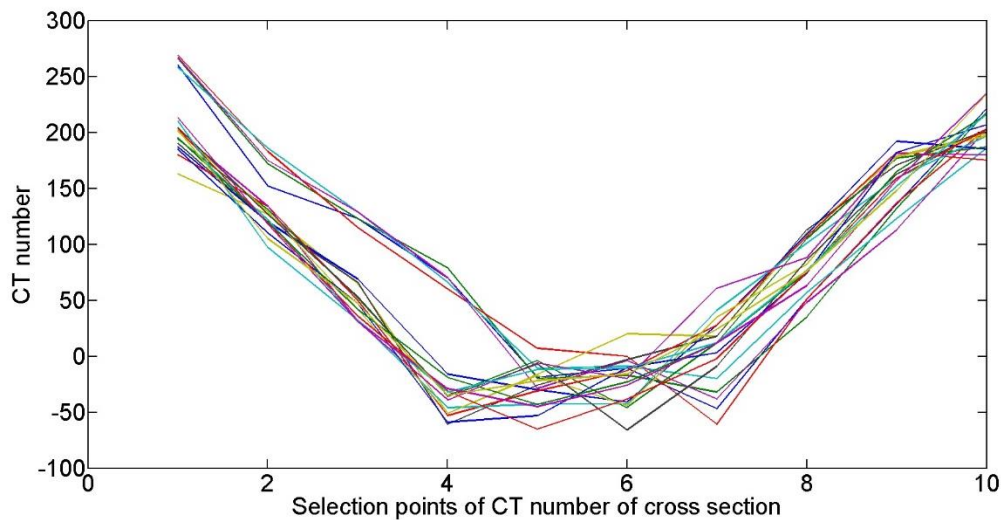


Fig. 7. Density distribution of fault planes of pine wood powder WPCs

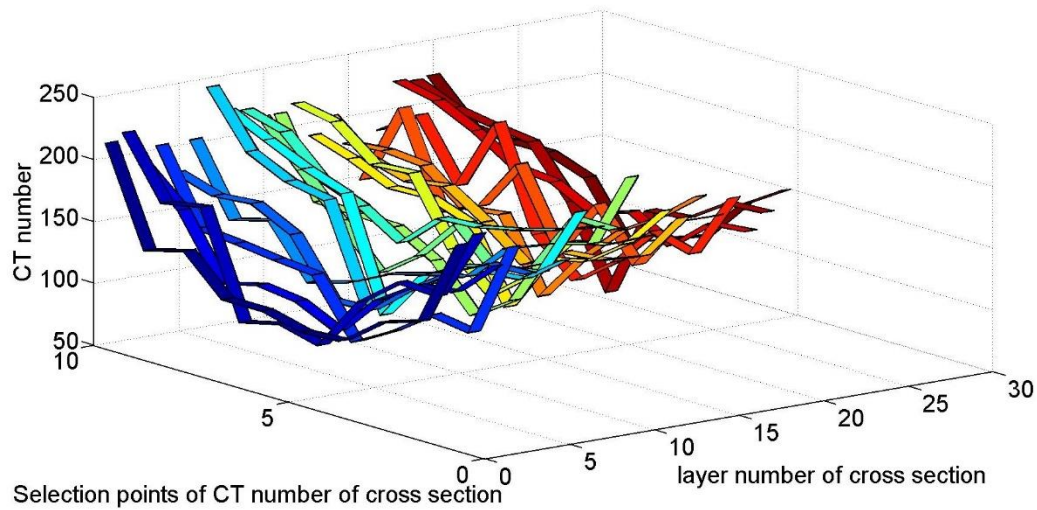


Fig. 8. Density spatial distribution of poplar powder WPCs

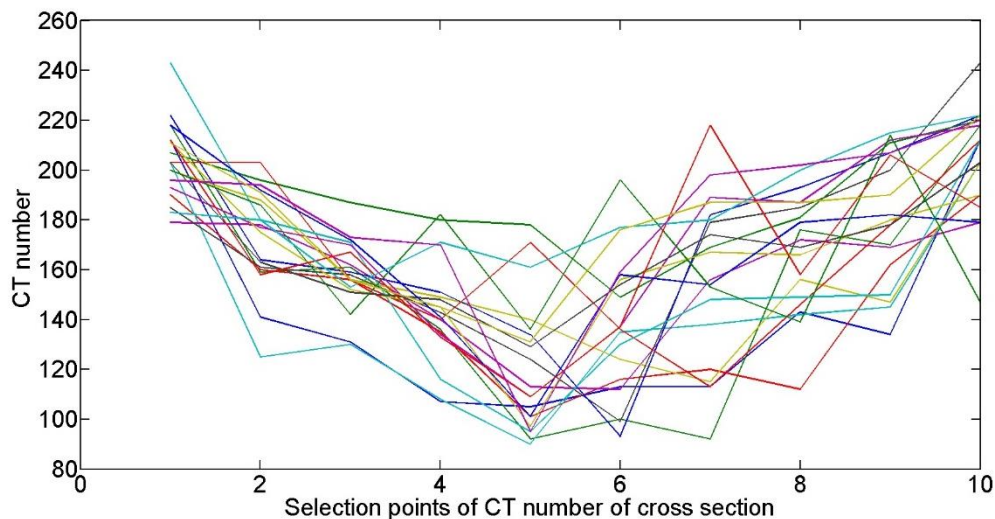


Fig. 9. Density distribution of fault planes of poplar wood powder WPCs

The average density distribution of 20-layer sections of two kinds of WPCs is exhibited in Fig. 10. Comparison shows that the density difference of pine wood powder WPCs was more apparent. That means that the density difference of poplar wood powder WPCs was small in the width direction of the plates, but their distributions both resembled a "V" shape. It should be mentioned that the edge densities of the two plates were approximately equal, but the density difference of the two plates gradually increased from the two edges to the middle in the width direction.

Density distribution of WPCs is directly related to the mechanical properties of WPCs; that is to say, the quality of WPCs products can be determined by the density distribution. However, the production process of both WPCs and raw materials will have an impact on the density distribution. Therefore, whether or not transverse fault density distribution characteristics of two kinds of selected WPCs represent all characteristics of WPCs is yet to be demonstrated by further experiments.

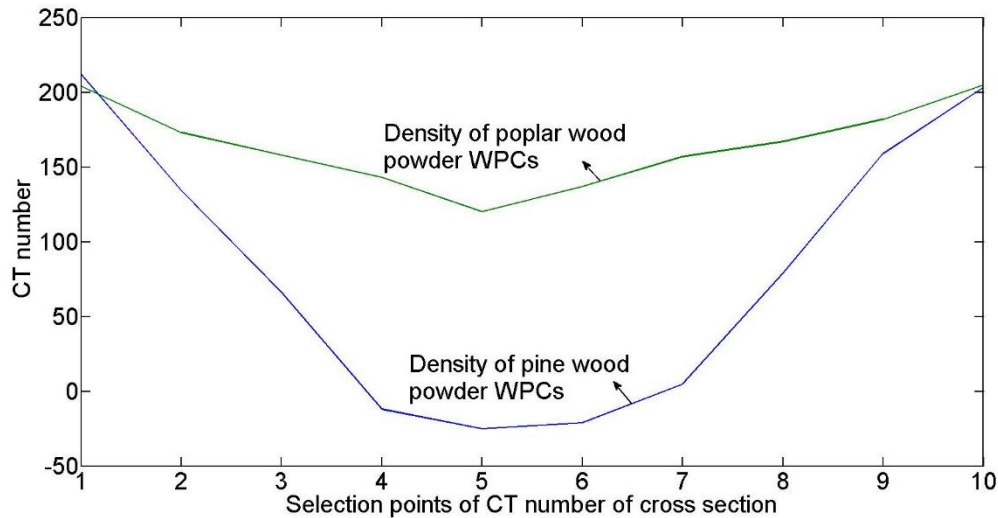


Fig. 10. Comparison of average density distribution of cross section

CONCLUSIONS

1. Based on the correlation among the attenuation coefficient, density, and CT number, a mathematical model between CT number and density of WPCs was established, which contributed to the realization of the fast and non-destructive detection of the density of WPCs and to the determination of the quality of WPC products.
2. Cross-sections of pine and poplar wood powder WPCs were scanned by CT. The cross-sectional density images were established. Cross sectional densities of pine and poplar powder WPCs changed greatly in the width direction. Density was high near the edge and was low in the middle, showing a "V" shape. A comparison of the results obtained for these two materials suggests that the density variation of pine powder WPCs was greater.

ACKNOWLEDGEMENTS

This work was financially supported by the Fundamental Research Funds for the Central Universities of China under Grant No. 2572014BB17, No.2572014CB30, the Project of the National Science Foundation of China (No. 31570712), the Project of the Natural Science Foundation of Heilongjiang Province of China (No.C201338), the Science and Technology Innovative Talents Special Funds Harbin (No.2012RFXXG080), and the Science and Technology Research Project of the Education Department of Heilongjiang Province (No.12543019).

REFERENCES CITED

- Adhikary, K. B., Pang, S. S., and Staiger, M. P. (2008). "Dimensional stability and mechanical behaviour of wood-plastic composites based on recycled and virgin high-density polyethylene (HDPE)," *Composites: Part B*. 39(5), 807-815. DOI: 10.1016/j.compositesb.2007.10.005
- Ashori, A. (2008). "Wood-plastic composites as promising green-composites for automotive industries!," *Bioresour. Technol.* 99(11), 4661-4667. DOI: 10.1016/j.biortech.2007.09.043
- Atanassov, K. T. (1983). "Intuitionistic fuzzy sets," *Seventh Scientific Session of ITKR* 11(6), 87-96.
- Bhandarkar, S. M., Luo, X. Z., Daniels, R., and Tollner, E. W. (2005). "Detection of cracks in computer tomography images of logs," *Pattern Recognit. Lett.* 26(14), 2282-2294. DOI:10.1016/j.patrec.2005.04.004
- Caufield, D. F., Clemons, C., and Rowell, R. M. (2010). *Wood Thermoplastic Composites. Sustainable Development in the Forest Products Industry*, Universidade Fernando Pessoa, Porto, Portugal.
- Clemons, C. (2002). "Wood-plastic composites in the United States: The interfacing of two industries," *Forest Prod J.* 52(6), 10-18, (<http://www.treearch.fs.fed.us/pubs/8778>).
- GB/T 17657 (1999). "Testing method for physical and chemical properties of artificial and decorative boards," China Standards Press, Beijing, China
- Khanjanzadeh, H., Tabarsa, T., Shakeri, A., and Omidvar, A. (2011). "Effect of organoclay platelets on the mechanical properties of wood plastic composites formulated with virgin and recycled polypropylene," *Wood Mater. Sci. Eng.* 6(4), 207-212. DOI: 10.1080/17480272.2011.606915
- Li, H. Y., Zhang, Z., Song, K. L., Lee, S., Chun, S. J., Zhou, D. G., and Wu, Q. L. (2014). "Effect of durability treatment on ultraviolet resistance, strength, and surface wettability of wood plastic composite," *BioResources* 9(2), 3591-3601. DOI: 10.15376/biores.9.2.3591-3601
- Petchwattana, N., Covavisaruch, S., and Sanetuntikul, J. (2012). "Recycling of wood-plastic composites prepared from poly (vinyl chloride) and wood flour," *Constr. Build. Mater.* 28(1), 557-560. DOI:10.1016/j.conbuildmat.2011.08.024
- Pritchard, G. (2004). "Two technologies merge: Wood plastic composites," *Reinf. Plast.* 48(6), 26-29. DOI: 10.1016/S0034-3617(04)00339-X
- Sarigul, E., Abbott, A. L., and Schmoldt, D. L. (2003). "Rule-driven defect detection in CT images of hardwood logs," *Comput. Electron. Agric.* 41(1-3), 101-119. DOI: 10.1016/S0168-1699(03)00046-2
- Stark, N. M., and Matuana, L. M. (2007). "Characterization of weathered wood-plastic composite surfaces using FTIR spectroscopy, contact angle, and XPS," *Polym. Degrad. Stab.* 92(10), 1883-1890. DOI:10.1016/j.polymdegradstab.2007.06.017
- TabkhPaz, M., Behraves, A. H., Shahi, P., and Zolfaghari, A. (2013). "Procedure effect on the physical and mechanical properties of the extruded wood plastic composites," *Polym. Compos.* 34(8), 1349-1356. DOI: 10.1002/pc
- Yang, N. X., and Qi, D. W. (2011). "Nondestructive testing of blockboard using combination of wavelet transform and gray-scale mathematical morphology," *Appl. Mech. Mater.* 55-57, 1206-1210. DOI:10.4028/www.scientific.net/AMM.55-57.1206

Yang, T. H., Yang, T. H., Chao, W. C., and Leu, S. Y. (2015). "Characterization of the property changes of extruded wood-plastic composites during year round subtropical weathering," *Constr. Build. Mater.* 88, 159-168. DOI:10.1016/j.conbuildmat.2015.04.019

Yu, X. E., and Lu, G.W. (2005). *The Principle, Structure and Quality Assurance of CT Device*, Science Press, Beijing, China.

Article submitted: August 23, 2015; Peer review completed: December 1, 2015; Revised version received: January 26, 2016; Accepted: February 20, 2016; Published: February 24, 2016.

DOI: 10.15376/biores.11.2.3538-3549